Applied Radiation and Isotopes 190 (2022) 110480

Contents lists available at ScienceDirect

Applied Radiation and Isotopes

journal homepage: www.elsevier.com/locate/apradiso

Half-life determination of ^{155}Tb from mass-separated samples produced at CERN-MEDICIS

S.M. Collins [a,b,*], A.P. Robinson [a,c,d], P. Ivanov [a], U. Köster [e], T.E. Cocolios [f], B. Russell [a], B. Webster [a,b], A.J. Fenwick [a], C. Duchemin [f,g], J.P. Ramos [f,g,h], E. Chevallay [g], U. Jakobsson [i,j], S. Stegemann [f], P.H. Regan [a,b], T. Stora [g]

[a] National Physical Laboratory, Hampton Road, Teddington, TW11 0LW, UK
[b] Department of Physics, University of Surrey, Guildford, GU2 7XH, UK
[c] Christie Medical Physics and Engineering (CMPE), The Christie NHS Foundation Trust, Manchester, M20 4BX, UK
[d] University of Manchester, Manchester, M13 9PL, UK
[e] Institut Laue-Langevin, 38042, Grenoble, France
[f] KU Leuven, Institute for Nuclear and Radiation Physics, Celestijnenlaan 200D, 3001, Leuven, Belgium
[g] CERN – European Organization for Nuclear Research, Esplanade des Particules 1, 1217, Meyrin, Switzerland
[h] Belgian Nuclear Research Centre SCK CEN, Boeretang 200, 2400, Mol, Belgium
[i] Helsinki Institute of Physics, University of Helsinki, 00014, Helsinki, Finland
[j] Department of Chemistry, University of Helsinki, 00014, Helsinki, Finland

A B S T R A C T

Terbium-155 has been identified for its potential for single-photon emission computed tomography (SPECT) in nuclear medicine. For activity measurements, an accurate and precise half-life of this radionuclide is required. However, the currently evaluated half-life of 5.32(6) d with a relative standard uncertainty of 1.1% determines the precision possible. Limited literature for the half-life measurements of this radionuclide is available and all reported investigations are prior to 1970. Further measurements are therefore needed to confirm the accuracy and improve the precision of the half-life for its use in the clinical setting. Two samples produced and mass separated at the CERN-MEDICIS facility have been measured at the National Physical Laboratory by two independent techniques: liquid scintillation counting and high-purity germanium gamma-ray spectrometry. A half-life of 5.2346(36) d has been determined from the weighted mean of the half-lives determined by the two techniques. The half-life reported in this work has shown a relative difference of 1.6% to the currently evaluated half-life and has vastly improved the precision.

1. Introduction

As part of the unique terbium radioisotope quartet (^{149,152,155,161}Tb) for molecular radiotherapy and diagnosis, ^{155}Tb has been proposed as a diagnostic component of this possible theranostic toolbox (Müller et al., 2012, 2014). The identical chemical characteristics and suitable physical half-lives of these terbium radioisotopes present an advantageous system as they can be linked to the same targeting vector providing the capability for unique theranostic treatment strategies and facilitating their application in personalised medicine (Müller et al., 2012). The in-vivo application of ^{155}Tb has been shown to provide excellent tumour visualisation at 24 h after injection and the half-life allowed additional longitudinal imaging with further imaging performed at 4 d after injection (Müller et al., 2012).

Terbium-155 (Q(ε) = 814.94(18) keV (Ge et al., 2022)) as a neutron-deficient isotope decays from its spin/parity $I^{\pi} = 3/2^{+}$ ground state via electron capture ($I\varepsilon$ = 100%) to excited states of the stable daughter nucleus ^{155}Gd. A proportion of decays goes directly to the spin/parity $I^{\pi} = 3/2^{-}$ ground state of the daughter ^{155}Gd (9%), with a higher probability of populating one of 22 previously reported excited levels. There are over 100 gamma transitions proposed that arise from the de-excitation of these excited states (Nica, 2019). The vast proportion of these transitions have a low emission probability of arising with only a small number of low-energy gamma-ray emissions (<200 keV) with significant intensities ($I\gamma > 1$ emission per 100 decays). A simplified decay scheme showing the significant gamma-ray emissions is shown in Fig. 1. The 86.6 keV ($I\gamma$ = 32.0(18) %) and 105.3 keV ($I\gamma$ = 25.1(13) %) gamma rays arising from the allowed Gamow-Teller decays to spin/-parity $5/2^{+}$ and $3/2^{+}$ states respectively are relatively well-suited for application in Single Photon Emission Computed Tomography (SPECT).

* Corresponding author. National Physical Laboratory, Hampton Road, Teddington, TW11 0LW, UK.
E-mail address: sean.collins@npl.co.uk (S.M. Collins).

https://doi.org/10.1016/j.apradiso.2022.110480
Received 4 August 2022; Received in revised form 20 September 2022; Accepted 20 September 2022
Available online 24 September 2022
0969-8043/© 2022 The Authors. Published by Elsevier Ltd. This is an open access article under the CC BY license (http://creativecommons.org/licenses/by/4.0/).

The diagnostic application of ^{155}Tb does not add a high radiation dose burden to the patient (Müller et al., 2012).

There is a scarcity of half-life determinations available in the current literature for ^{155}Tb (Table 1), with only two measurements that quote an uncertainty and no half-life investigations reported since 1970. The determinations made by Toth et al. (1960) and Chu et al. (1970), in common with this work, measure samples that have been chemically and mass separated. However, neither provide any details of any residual contaminants and they both share a common lack of documented analysis of the uncertainty components, in cases where a standard uncertainty has been reported. The currently evaluated half-life of 5.32(6) d (Nica, 2019) has been derived exclusively from the Ge(Li) gamma-ray spectrometry measurements by Chu et al. (1970).

To provide a foundation for future pre-clinical and clinical trials of this radionuclide there is a need for absolute standards of activity and improved nuclear data. However, the relative standard uncertainty of 1.1% associated with the half-life of ^{155}Tb represents a significant hindrance to the provision of a precise absolute activity standard. Thus, there is a clear need to verify and improve upon the currently accepted half-life, with the inclusion of a robust and documented uncertainty estimation.

In this work, two independent radiometric techniques have been used: liquid scintillation counting (LSC) using the Triple-to-Double Coincidence Ratio (TDCR) method and high-purity germanium (HPGe) gamma-ray spectrometry techniques to observe the decay rate of ^{155}Tb. Two samples of ^{155}Tb have been used (henceforth, referred to as sample 1 and sample 2), which have been produced and mass-separated at the CERN-MEDICIS facility (Duchemin et al., 2020, 2021; Palenzuela et al., 2021).

Table 1
Table of literature values for the half-life of ^{155}Tb.

Reference	Year	$T_{1/2}$ /d	$u(T_{1/2})$ /%	Comments
Mihelich et al.	1957	5.6 (–)	–	–
Toth et al.	1960	5.4 (2)	3.7	Proportional counter; Mass separated
Chu et al.	1970	5.32 (6)	1.1	Gamma-ray spectrometry of the 86.6 keV and 105.3 keV full-energy peaks; Mass separated; four determinations were made.

2. Methodology

2.1. Fitting of the observed decay rate

The temporal behaviour of the observed decay rate where only one radionuclide is under observation can be determined using a weighted non-linear least-squares fit to the standard relation for single component radioactive decay:

$$A_t = A_0 k e^{-\lambda t} \tag{1}$$

where A_t and A_0 are the activity of the radionuclide at time t and $t = 0$ respectively, λ is the decay constant of the radionuclide. The correction factor k accounts for decay during the measurement where:

$$k = \frac{(1 - e^{-\lambda \Delta t})}{\lambda \Delta t} \tag{2}$$

where Δt is the duration of the measurement.

In any half-life measurement campaign where Eq. (1) is true then it can be assumed that components to derive the activity, such as the

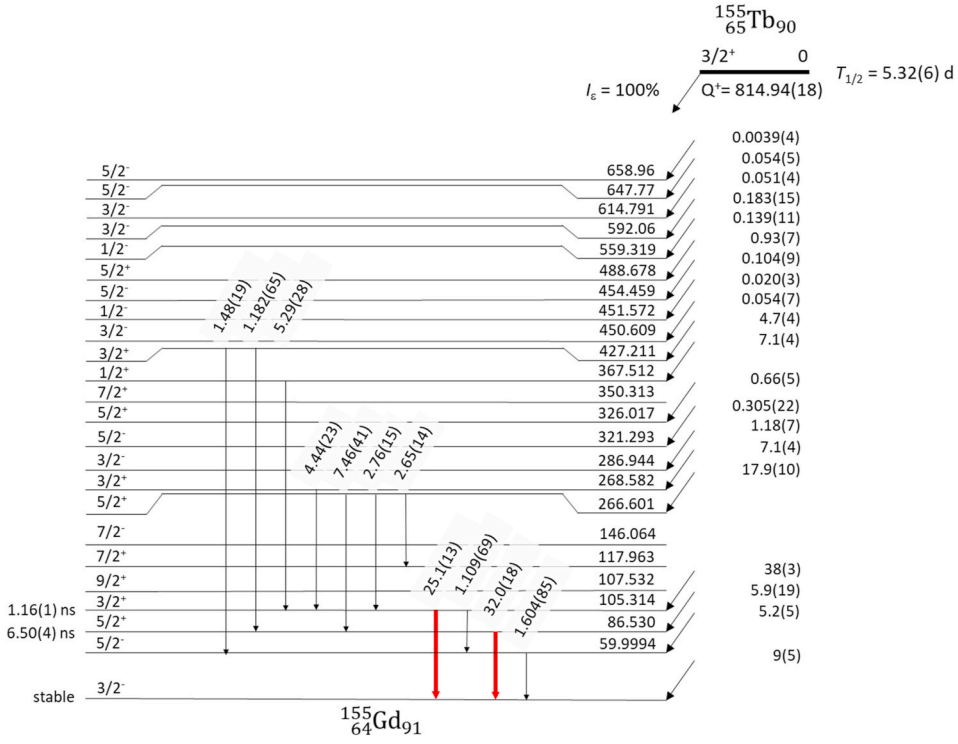

Fig. 1. *Simplified decay scheme of ^{155}Tb showing the gamma-ray emissions where Iγ > 1 per 100 decays (Nica, 2019; Ge et al., 2022). The absolute intensities for these gamma-ray emissions are included. The 86.6 keV and 105.3 keV gamma-ray emissions used in the half-life determination in the current work are shown as red arrows.* (For interpretation of the references to colour in this figure legend, the reader is referred to the Web version of this article.)

counting efficiency or absolute gamma-ray emission intensities, are common across all measurements and can therefore be neglected. Thus, the activity of the sample can be represented by the observed count rate.

In the case of the decay of the activity of two or more radionuclides being observed simultaneously, for example where contaminants are present (Collins et al., 2015; Bobin et al., 2019), the temporal behaviour of the total activity can be represented by a sum of two or more exponentials. Eq. (1) is expanded to include each additional radionuclide such as:

$$A_t = B_{0,1}k_1e^{-\lambda_1 t} + B_{0,2}k_2e^{-\lambda_2 t}\ldots + B_{0,i}k_ie^{-\lambda_i t} \tag{3}$$

where A_t is the sum of the activity of all radionuclides at time t and $B_{0,i}$ a response value for the ith radionuclide at $t = 0$ respectively.

An estimate of the half-life of the principal radionuclide can then be obtained from a non-linear least-square fit of Eq. (3) to the measured data points of the dataset. Using fixed values for λ of any radionuclide contaminant and by iterative refinement of parameters $B_{0,i}$ and λ of the principal radionuclide the maximum likelihood estimate of the half-life is determined through the minimisation of the reduced $\chi 2$:

$$\frac{\chi^2}{\upsilon - 1} = \sum \left(\frac{x_{obs} - f(x)}{\sigma_{obs}}\right)^2 \tag{4}$$

where x_{obs} and σ_{obs} are the measured data points and standard uncertainty for each data point respectively.

2.2. Uncertainty of the half-life

The uncertainty components of the half-life were evaluated in accordance with the proposed methodology in Pommé (2015), where the relative uncertainty of the activity from the considered uncertainty component, $\sigma(A)/A$, are defined by their frequency of occurrence in the measured dataset (i.e. low-, medium- and high-frequency).

The propagation factors for the high-frequency deviation uncertainty component are derived from the formula (Pommé and De Hauwere, 2020)

$$\frac{\sigma(T_{1/2})}{T_{1/2}} = \frac{2}{\lambda T}\sqrt{\frac{3(n-1)}{n(n+1)}}\,\frac{\sigma(A)}{A} \tag{5}$$

where λ is the decay constant, T is the duration of the measurement campaign and n is the number of measurement data. This propagation formula is robust where the occurrences of the uncertainty component are performed equidistant in time over the measurement campaign. In practice, this method also provides a relatively robust approximation where data sets loosely comply with this condition (Pommé and De Hauwere, 2020).

Medium-frequency components have been investigated by way of an empirical mode decomposition algorithm applied to the residuals of the least-squares fit (Pommé and Pelczar, 2021), which has been used to extract observable and hidden structures from the random statistical component. These are decomposed into modes, where the first mode, C_1, is the random statistics, with the additional modes representing the medium-frequency deviations. A hypothetical bias to the half-life has been calculated as a function of time for each mode, with an envelope uncertainty function covering the absolute values of the biases over the measurement campaign.

The low-frequency deviations have been assessed from those components that apply across the full measurement campaign and are invisible within the residuals. These are identified for each technique later, but may include linearity of the detector response, background corrections, dead time and pulse pile-up corrections, radionuclide contaminant corrections. The propagation formula for these components is calculated using (Pommé, 2015):

$$\frac{\sigma(T_{1/2})}{T_{1/2}} \approx \frac{2}{\lambda T}\left\langle\frac{\sigma(A)}{A}\right\rangle \tag{6}$$

2.3. HPGe gamma-ray spectrometry

Two p-type HPGe gamma-ray spectrometers were used at the National Physical Laboratory (NPL) to perform the half-life measurements, activity, and contaminant assay. For sample 1, a 22% relative efficiency detector (identified as LOKI) with a measured energy resolution (FWHM) of 0.678 keV and 0.702 keV at 86.6 keV and 105.3 keV respectively was used. For sample 2, a 9.5% relative efficiency detector (identified as THOR) and measured energy resolution of 0.677 keV and 0.704 keV at 86.6 keV and 105.3 keV respectively was used. These detectors had been previously calibrated for their full-energy peak (FEP) detection efficiency for the geometry and chemical matrices used in this work. This was determined using a suite of traceable primary and secondary gamma-ray emitting radionuclide standards covering the photon energy range 60 keV–1836 keV.

Both detectors were contained in Pb shields comprised of 10 cm thick Pb walls covered with 0.5 mm Cd and 0.7 mm Cu graded liner to reduce effects from background radiation and Pb fluorescence X-rays in the spectra. Aluminium optical breadboards were mounted in line with the detector along the horizontal plane with a kinematic mounting plate holding a precision-engineered sample holder to provide highly reproducible geometric source positioning.

The spectra for both detectors were collected using a CANBERRA LYNX digital signal analyser (DSA) connected to a PC running CANBERRA GENIE 2000 v3.4.1. All spectra were collected using the loss-free counting option in the DSA, which had previously been validated to correct for dead time and pulse pile-up to within 0.10% over the range of count rates observed. The detection efficiency stability of the two HPGe gamma-ray spectrometers has been monitored at weekly intervals over their operational lifetime using a ^{152}Eu source. The uncertainty for the detection efficiency stability from these measurements has been estimated at 0.10%.

2.4. Liquid scintillation counting

The liquid scintillation counting was performed using a Hidex 300SL, which is an automatic system that incorporates three photomultiplier tubes (PMTs) that allows for the use of the triple-to-double coincidence (TDCR) counting technique. This technique has advantages as it provides a method for determining the counting efficiency from the TDCR parameter from the triple count rates, R_T, and double count rates, R_D (TDCR = R_T/R_D) when applying the "free parameter model" (Broda et al., 2007; Grau Malonda, 1999). A temporally stable counting efficiency is therefore related to a temporally stable TDCR parameter (Kossert et al., 2020). The observed change of the TDCR parameter over the course of the measurement campaign for sample B is shown in Fig. 2. The linearity of the Hidex 300SL has previously been assessed using a ^{18}F source that covered the count rates observed in this work. The linearity uncertainty was estimated as 0.10%.

The three ^{155}Tb vials were placed sequentially with a background vial at either end, which were automatically measured in sequence over the course of the measurement campaign. For each measurement of the background and active vials the HIDEX 300SL provides the logical sum of doubles counts, from which the half-life has been determined, and the measured TDCR value. The background count rate for both background vials throughout the measurement campaign had a standard deviation of 5%.

The logical sum of doubles count rate, R_D, for each datum was determined using:

$$R_D(t) = \frac{N_D - B_D}{\Delta t}k_\tau \tag{7}$$

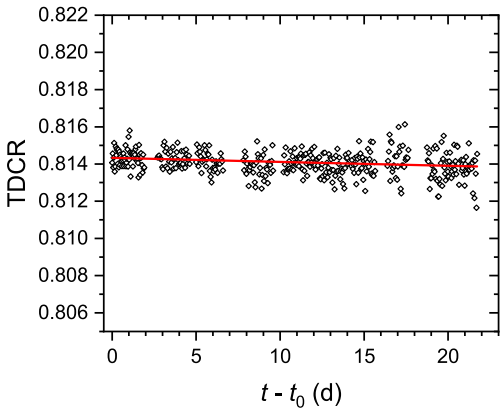

Fig. 2. The observed TDCR parameter throughout the measurement campaign for sample B. The trend of the TDCR parameter observed presented is representative of the trend across all three samples.

where N_D is the logical sum of double counts observed in the counting period, Δt, B_D is the average of the background count rate taken on either side of the measurement, and k_r is the correction for the dead time.

2.5. Production and preparation

2.5.1. Sample 1

The ^{155}Tb was produced and collected at the CERN-MEDICIS facility and produced during the MED004 approved experiment. A high-purity Ta metal target (*Ta647M, 99.95% purity*) was irradiated in the High-Resolution Separator (HRS) target station beam dump position at ISOLDE. This target was located downstream of a primary HRS target made of SiC (*623SiC*, ISOLDE physics program) and received a fraction of the scattered 1.8×10^{18} 1.4 GeV protons from the Proton Synchrotron Booster accelerator at CERN. The irradiated target was moved to the CERN-MEDICIS isotope mass separator to release and extract ion species selected at a mass-to-charge ratio of 155 (Cavaier et al., 2017). The mass-separated ion beam was implanted with 30 keV into a Zn-coated Au foil on September 29, 2017. The following radionuclides, implanted as isobars (same mass-to-charge ratio), and nominal activities (A) were present on the Zn/Au foil at the time of implantation: $A(^{139}\text{Ce}) = 6.9$ MBq (implanted as $^{139}\text{Ce}^{16}\text{O}^{+}$); $A(^{155}\text{Dy}) = 3.6$ MBq; $A(^{155}\text{Tb}) = 20$ MBq.

The target foil was delivered to NPL on October 2, 2017. To maximise the yield of ^{155}Tb, the Zn layer was dissolved in 20 mL 6 mol dm^{-3} HCl, and the Au foil containing part of the ions traversing the Zn layer was dissolved in 20 mL *aqua regia*. The two solutions were combined and evaporated to incipient dryness. This was re-dissolved in 10 mL of a mixture of 8 mol dm^{-3} HNO_3 and 0.1 mol dm^{-3} $NaBrO_3$ oxidant. The ^{155}Tb was isolated from the ^{139}Ce using the UTEVA resin-based separation method described in Webster et al. (2019). This provided a resulting solution of nominal activity 3.8 MBq at 2017-10-04 12:00 UTC in approximately 5 mL 1 mol dm^{-3} HCl. A 1 g aliquot of this solution was dispensed to a 2 mL ISO ampoule for measurement by HPGe gamma-ray spectrometry (ISO, 2010). The activity of ^{155}Dy ($T_{1/2} = 9.9(2)$ h (Nica, 2019)) was negligible by the time of measurement at NPL and had decayed below the detection limit for ^{155}Dy (1.75 kBq).

2.5.2. Sample 2

A second sample of ^{155}Tb with a nominal activity of 4 MBq was delivered to NPL on July 22, 2020. This sample was produced at the ARRONAX cyclotron (Nantes, France) from the irradiation of a natural Gd foil (99.9% purity) with 34 MeV protons on July 13, 2020. This irradiation can result in the co-production of other Tb radioisotopes from the ^{nat}Gd(p,xn) reaction and thus an additional isotope mass separation step is needed to provide ^{155}Tb at high radionuclidic purity (Formento-Cavaier et al., 2020). However, before mass-separation, the irradiated Gd foil was dissolved and radiochemically processed using an LN resin method, this increased the Tb:Gd ratio from 1:100000 to 1:100 and suppressed any non-Tb contaminants (Webster, 2021). The processed solution was deposited and evaporated on a dedicated sample holder developed at CERN, to transfer the radioactive source rapidly and securely into the empty target tantalum oven of a standard ISOLDE/MEDICIS target.

To extract ^{155}Tb, the target unit 671 M containing the oven and equipped with a Rhenium ion source at 2000 °C was installed in the MEDICIS isotope separator. The sample was heated to 2200 °C and laser resonance ionisation was applied using the MEDICIS Laser Ion Source for Separator Assembly (MELISSA) to selectively enhance the ionisation of ^{155}Tb (Gadelshin et al., 2020). The mass separated ^{155}Tb beam was implanted at 30 keV into a Zn-coated Au foil on 15–17 July 2020.

On delivery at NPL, the radionuclides present in the Zn layer were recovered by dissolution in 10 mL 6 mol dm^{-3} HCl. The solution underwent a further separation on LN resin to remove any potential impurities (Webster, 2021). The separated solution was evaporated to dryness before being re-dissolved in 2 mL 0.1 mol dm^{-3} HCl. From this, a 0.75 g aliquot was dispensed to a 2 mL ISO ampoule for contaminant check by HPGe gamma-ray spectrometry, and 0.02 g aliquots were dispensed to each of three Perkin Elmer Plastic Scintillation vials containing 10 mL of Ultima Gold AB scintillation cocktail for measurement of the half-life.

2.6. Activity and contaminant determination

2.6.1. Sample 1

After the chemical separation the resulting sample was measured by the HPGe gamma-ray spectrometer LOKI (see section 2.1) for 7.2×10^3 s on October 4, 2017 at a source-to-detector distance of 295 mm. No gamma-ray emitting contaminants were detected. The activity of the ^{155}Tb and detection limits (DL) of the possible contaminants ^{139}Ce, ^{154}Tb and ^{156}Tb at the reference time 2017-09-29 12:00 UTC are provided in Table 2.

2.6.2. Sample 2

The sample prepared for contaminant check was measured by the HPGe gamma-ray spectrometer THOR for approximately 2.35×10^5 s at a source-to-detector distance of 150 mm. The spectrum is presented in Fig. 3. In addition to the expected FEPs associated with the decay of ^{155}Tb, the presence of ^{156}Tb was identified ($A_0(^{156}\text{Tb})/A_0(^{155}\text{Tb}) = 3.25(38) \times 10^{-4}$) which results from a high-mass tailing interference in the mass separation process. The activity determined for the ^{155}Tb and ^{156}Tb are given in Table 3. The detection limit for ^{154}Tb is also provided in Table 3 as an indication of the low-mass tailing interference in the mass separation process. The ratio of the number of atoms (N) of ^{154}Tb and ^{156}Tb to ^{155}Tb is given in Table 3 to provide an indication of the low- and high-mass tailing.

Europium-155 ($T_{1/2} = 4.753(14)$ a (Bé et al., 2004)), which also

Table 2
Activity per unit mass of the ^{155}Tb and the detection limit of ^{139}Ce, ^{154}Tb and ^{156}Tb in Sample 1 at the reference time of 2017–09-29 12:00 UTC. The half-lives have been taken from various sources as referenced.

Radionuclide	$T_{1/2}$	*Reference*	A_0 /kBq g^{-1}	DL_0(Imp)/ $A_0(^{155}\text{Tb})$
^{139}Ce	136.641(20) d	Bé et al. (2008)	DL = 0.30	2.1×10^{-4}
^{154}Tb	21.5(4) h	Reich (2009)	DL = 6.5	4.5×10^{-3}
^{155}Tb	5.2346(36) d	This work	1456(12)	–
^{156}Tb	5.35(10) d	Reich (2012)	DL = 0.093	6.4×10^{-5}

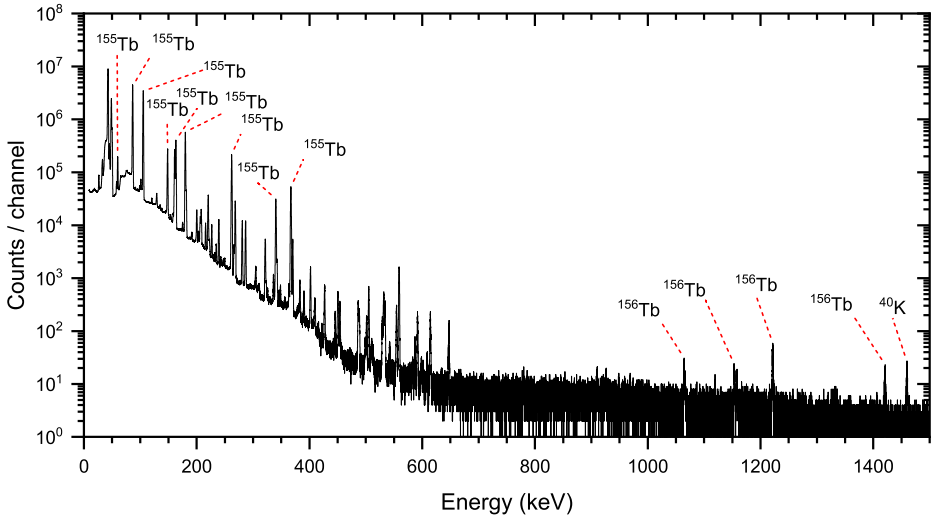

Fig. 3. HPGe gamma-ray spectrum of ^{155}Tb source collected for 2.35 × 10^5 s on July 24, 2020 at a source-to-detector distance of 150 mm. The main emissions of ^{155}Tb (Iγ > 1%) have been annotated along with the emissions of the ^{156}Tb contaminant. The remaining unidentified peaks are associated with the decay of ^{155}Tb.

Table 3
Activity per unit mass of the ^{155}Tb and ^{156}Tb and the detection limit of ^{154}Tb in Sample 2 at the reference time of 2020-07-22 12:00 UTC. The ratio of the number of atoms at the reference time, N_0, of the contaminants (Imp) to the ^{155}Tb is also shown. The half-lives have been derived from various sources as referenced.

Radionuclide	$T_{1/2}$	*Reference*	A_0 kBq g^{-1}	A_0(Imp)/ A_0(^{155}Tb)	N_0(Imp)/ N_0(^{155}Tb)
^{154}Tb	21.5(4) h	Reich (2009)	DL = 0.24	6.3 × 10^{-4}	1.07 × 10^{-4}
^{155}Tb	5.2346 (36) d	This work	383.6 (44)	–	–
^{156}Tb	5.35 (10) d	Reich (2012)	0.125 (14)	3.25(38) × 10^{-4}	3.33 × 10^{-4}

decays to the ground state of ^{155}Gd by beta-minus decay, shares the same major characteristic gamma rays of the excited states of ^{155}Gd at 86.6 keV and 105.3 keV (Bé et al., 2004). Europium-155 can be produced in the collection foil by ^{156}Gd(p,2p), ^{157}Gd(p,^{3}He), ^{158}Gd(p,α) and ^{160}Gd(p, α2n) reactions. The sample underwent radiochemical separation to suppress contaminants, including ^{155}Eu, at the ARRONAX facility and again at NPL. Whilst this would be considered more than sufficient to provide a sample sufficiently clean of all non-terbium isotopes a further measurement was made at the end of the measurement campaign (after approximately four ^{155}Tb half-lives) by HPGe gamma-ray spectrometry. The sample was re-measured for approximately 2.3 × 10^5 s in the same geometry. No deviation was observed of the decay corrected activity of ^{155}Tb to the initial measurement using the 86.6 keV and 105.3 keV gamma rays. The decay correction was performed using the half-life determined in this work. This indicates that any ^{155}Eu activity present was negligible throughout the measurement campaign. Furthermore, no radionuclides which may have been obscured at the higher ^{155}Tb activity were identified.

3. Results

3.1. HPGe gamma-ray spectrometry

A total of 143 spectra were collected over a period of 18.6 d (~3.55 half-lives) commencing on October 4, 2017. The spectra were collected for periods ranging from 7.2 × 10^3 s at the start of the measurement campaign and extended to 1.05 × 10^4 s towards the end of the measurement campaign. This ensured that peak areas of more than 4 × 10^5 counts were collected throughout. For each spectrum, the 86.6 keV and 105.3 keV FEPs were fitted using an NPL developed Microsoft Excel-based software package (Collins et al., 2020). Examples of these fits for each FEP are shown in Fig. 4. The count rates of the 86.6 keV and 105.3 keV net peak areas were respectively 606.5 s^{-1} and 498.3 s^{-1} at the start of the campaign and approximately 52.0 s^{-1} and 42.8 s^{-1} at the end of the campaign.

Since no impurities were detected, the weighted non-linear least-square fit to the 86.6 keV and 105.3 keV datasets was performed using Eq. (1). The weight component for each datum was composed of the combined uncertainty of the net peak area statistics and continuum subtraction. The net peak area statistical component was the dominant component throughout for both datasets with the statistical component and continuum component at the start of the campaign being 0.053% and 0.020% respectively and 0.15% and 0.056% for the final measurement of the 105.3 keV dataset and similar for the 86.6 keV dataset.

The least-squares fit and residuals, as relative differences, to each gamma-ray energy dataset are shown in Fig. 5. From the residuals, there was observed an anomalous set of data at ($t - t_0$) = 14 d–14.5 d. Whilst these data agree, within two standard uncertainties, they show a trend that stands out from the rest of the dataset in both gamma-ray emissions. From the analysis of the data, no reason could be identified for this anomaly. The rejection of these data leads to a relative increase of the

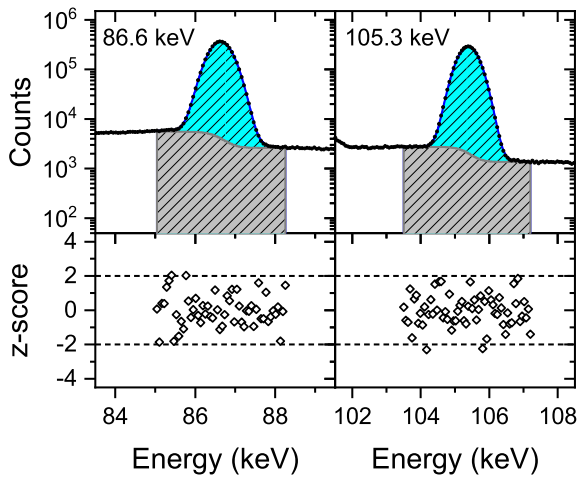

Fig. 4. Fits of the 86.6 keV (Left) and 105.3 keV (Right) full-energy peaks from the first spectrum collected for 7.2 × 10^3 s.

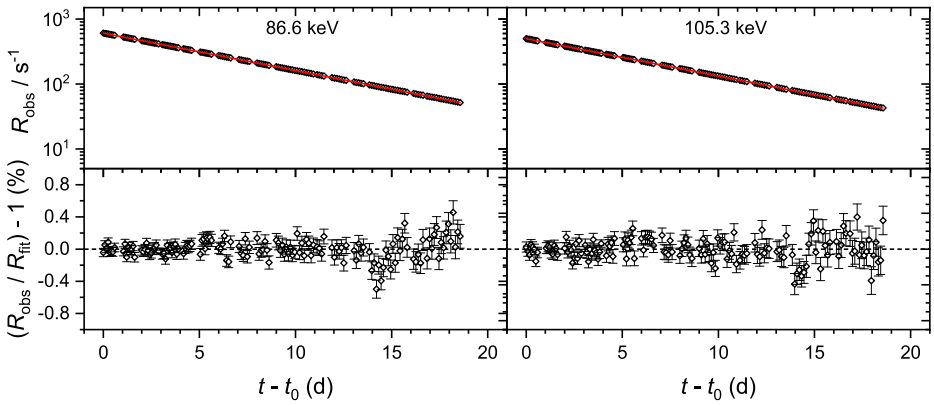

Fig. 5. The least-squares fit to the observed rates (top) and the relative residuals of the fits (bottom) for the 86.6 keV (left) and 105.3 keV (right) datasets.

half-life by 0.017%. Ultimately, the combined standard deviation of the half-life is more than sufficient to cover this difference.

Empirical decomposition was applied to the two datasets, extracting the random statistical mode (C_1), an underlying medium-frequency mode (C_2) and a slower oscillation (C_3) (Fig. 6). The anomalous region around day 14 was extracted into C_2. The bias to these modes as a function of time and the envelope uncertainty function was calculated (Fig. 7). The envelope uncertainty components for C_2 and C_3 have been included in the final uncertainty budget for each gamma-ray energy (Table 4). For the 105.3 keV, the random statistical uncertainty calculated from the standard deviation of the residuals using Eq. (5) is similar to C_1. However, for the 86.6 keV, C_1 is about half that calculated with Eq. (5). To avoid any underestimation of the uncertainty, the uncertainty propagated from the standard deviation of the residuals has been used.

The low-frequency components were identified as the dead time and

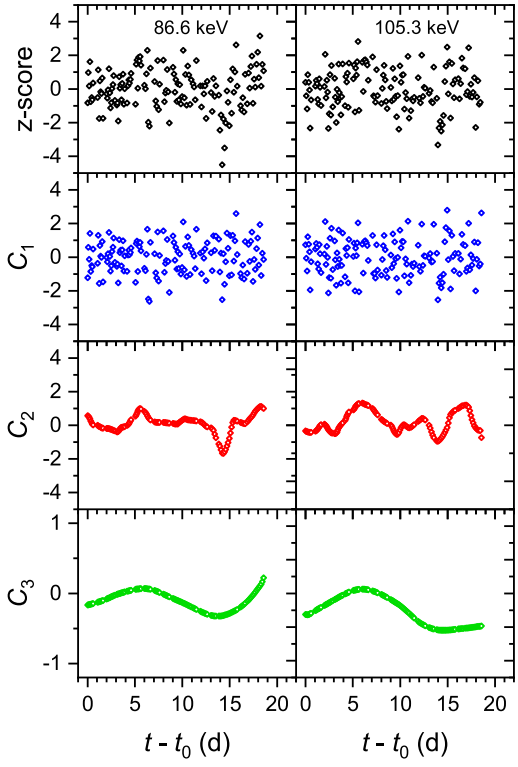

Fig. 6. *Empirical mode decomposition of the residuals to the least-squares fit of the 86.6 keV (left) and 105.3 keV (right) data sets measured by HPGe gamma-ray spectrometry. The random statistical component (C_1), a medium-frequency component (C_2), and a slower oscillation (C_3) are shown.*

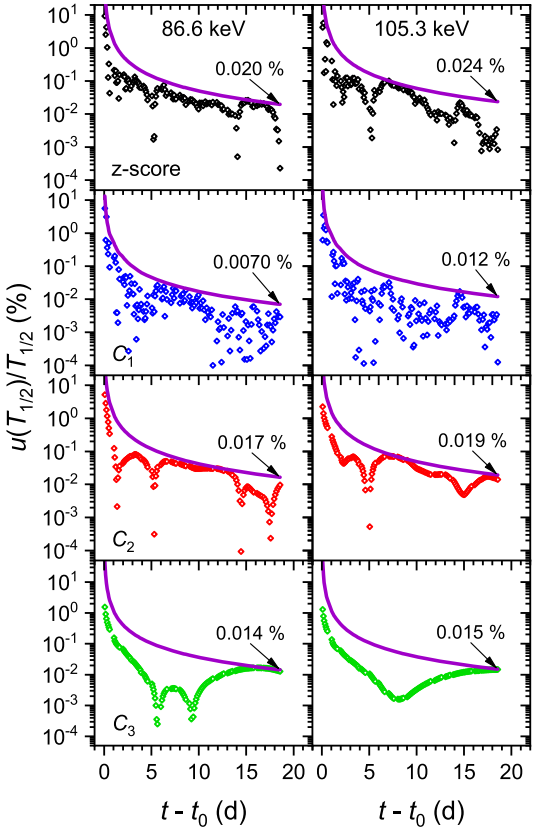

Fig. 7. *The relative uncertainty of the half-life for the decomposition modes C_1, C_2 and C_3 as a function of time for the 86.6 keV (left) and 105.3 keV (right) residuals. The purple line represents their envelope function, with their ultimate uncertainty values indicated.* (For interpretation of the references to colour in this figure legend, the reader is referred to the Web version of this article.)

pulse pile-up (i.e. linearity), detection efficiency stability, and peak fitting and continuum subtraction. The $u(A)/A$ for the linearity and detection efficiency stability have already been specified in section 2.3. These linearity and stability components were correlated across both gamma-ray emissions and thus combined in quadrature into the final uncertainty.

The FEP area and continuum fitting component was estimated for each gamma-ray transition by varying the region of interest around the FEP and redetermining the half-life. The uncertainty was derived from the range of half-lives determined. The effect of changing the ROI was found to be relatively small, with values of approximately 0.025% determined for each gamma-ray energy.

Table 4
The half-life and uncertainty budget for HPGe gamma-ray spectrometry of sample 1.

Component	86.6 keV				105.3 keV			
	$\frac{\sigma(A)}{A}$	n	Propagation Factor	$\frac{\sigma(T_{1/2})}{T_{1/2}}$	$\frac{\sigma(A)}{A}$	n	Propagation factor	$\frac{\sigma(T_{1/2})}{T_{1/2}}$
	/%			/%	/%			/%
Random statistics	0.12	143	0.117	0.014	0.12	143	0.117	0.014
Medium frequency (C_2)	–	–	–	0.017	–	–	–	0.019
Slow oscillation (C_3)	–	–	–	0.014	–	–	–	0.015
FEP fitting/Continuum subtraction	–	–	–	0.025	–	–	–	0.026
$T_{1/2}$/gamma-ray emission	5.2343(19) d			0.036	5.2356(20) d			0.039
Standard uncertainty of weighted mean	–	–	–	0.026				
Detection efficiency stability	0.10	1	0.8138	0.081				
Linearity (dead time/pulse pile-up)	0.10	1	0.8138	0.081				
$T_{1/2}$	5.2349(62) d			0.12				

The half-life determined for each gamma-ray emission dataset and the standard uncertainty determined from the statistical, C_2, C_3, and FEP fitting component are provided in Table 4. The final half-life was determined from the weighted mean of the two gamma-ray emissions, using the combined uncertainty of the statistical, C_2, C_3, and FEP fitting component to provide the weight factor, and including the additional correlated low-frequency components was $T_{1/2}(^{155}\text{Tb}) = 5.2349(62)$ d.

3.2. Liquid scintillation counting – sample 2

The three vials were measured with a total of 413 repeats over a period of 21.7 d (approximately 4.2 half-lives) commencing on July 23, 2020. The net count rate R_D (Eq. (7)) for each sample were approximately 4700 s^{-1} and 270 s^{-1} at the start and end of the measurement campaign. The average background count rate over the campaign was 0.684 s^{-1}.

The presence of ^{156}Tb had been identified and quantified by HPGe gamma-ray spectrometry, therefore Eq. (3) was used to fit the acquired datasets. The activity of the ^{156}Tb was fixed as the activity ratio as determined in section 2.6.2 corrected to the start of the measurement campaign. The presence of the ^{156}Tb had an unobservable effect in the observed activity over time, due to its low starting activity and similar half-life to ^{155}Tb. However, as the ^{156}Tb can be accounted for in the decay curve, the effect of the impurity on the half-life is negligible throughout as seen in the uncertainty propagation in Fig. 8. In Fig. 9, the least-squares fit to the datasets and their residuals, as relative differences, are shown.

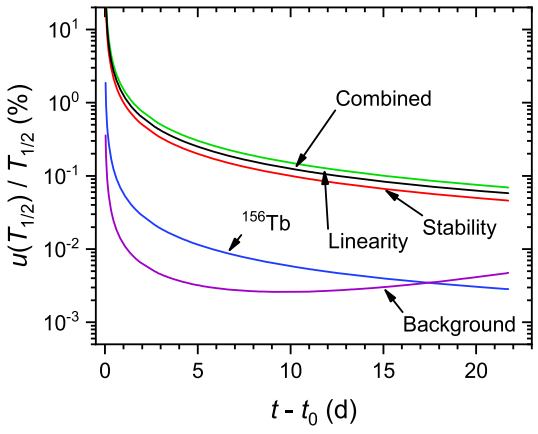

Fig. 8. Evolution of the propagated low-frequency uncertainty components of the half-life with time.

The residuals of each sample dataset were analysed by empirical decomposition, extracting the random statistical (C_1), medium-frequency (C_2), and slow-frequency (C_3) modes (Fig. 10). The envelope uncertainty was calculated for each mode and an ultimate uncertainty was determined for each (Fig. 11). For each sample, the C_1 uncertainty agreed well with the standard deviation of the residuals using Eq. (5). Multiple fluctuations throughout the campaign were observed in the C_2 mode, which results in an additional uncertainty component between 0.011% and 0.020%. These fluctuations may be caused by short-term changes in the counting efficiency of the detector system. The repositioning of the samples was identified as a possible component but neglected as $n = 413$ and was therefore considered negligible. The slow-frequency fluctuation in the C_3 mode identified in each dataset may be indicative of the long-term fluctuations in the stability and linearity of the detection system. For Sample A and B the value of this component is relatively small to that of C_2, whilst for Sample C it about the same magnitude as C_2. However, the magnitude of the additional uncertainty for this component may be suppressed due to the minimisation effects of the least-squares fit.

The half-life determined from each sample dataset and an uncertainty composed of the random and medium frequency components summed in quadrature is given in Table 5. The final half-life of ^{155}Tb by liquid scintillation counting was derived from the weighted mean of the three determinations.

All three sample datasets share the same low-frequency deviation components, which were combined in quadrature with the standard uncertainty of the weighted mean to derive the standard uncertainty of the half-life. These were identified as the stability, linearity, ^{156}Tb contaminant, and background.

The stability uncertainty has been taken from the relative change of the TDCR parameter from the start to the end of the measurement campaign. The uncertainty for this stability component was estimated from the relative difference of the start and end point of a linear fit to the TDCR values of the three samples measured. A value of 0.066% was estimated for the uncertainty of the stability component. As an alternative method, the half-life was determined using the R_D corrected by the calculated TDCR value for each measurement. The half-life determined for each sample was found to be approximately 0.02% longer. This relative difference found between the half-life determined for the R_D and the TDCR-corrected R_D is covered by the $u(T_{1/2})/T_{1/2}$ for the stability component (Table 5). As ^{155} Tb decays purely by electron capture, the effects of quenching, brought about by the degradation of the scintillation cocktail over time may result in the counting efficiency not being directly related to the observed TDCR parameter as the

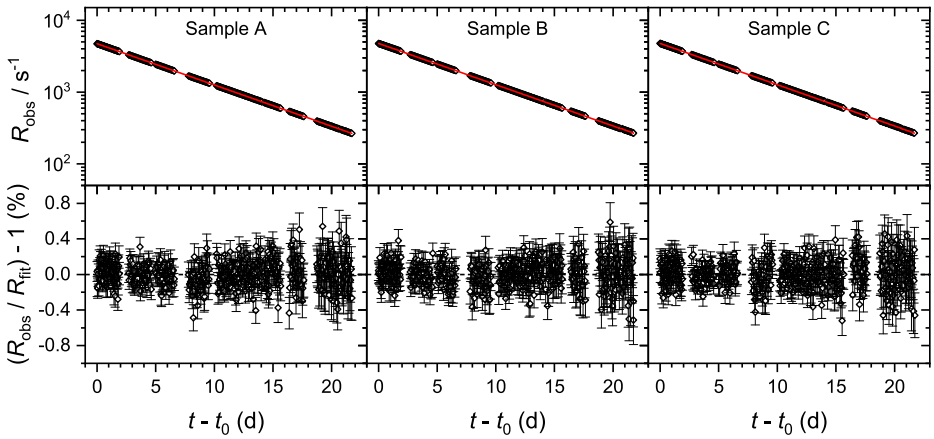

Fig. 9. The least-squares fit to the observed R_D (top) and the relative residuals of the fits (bottom) for the samples A, B, and C datasets.

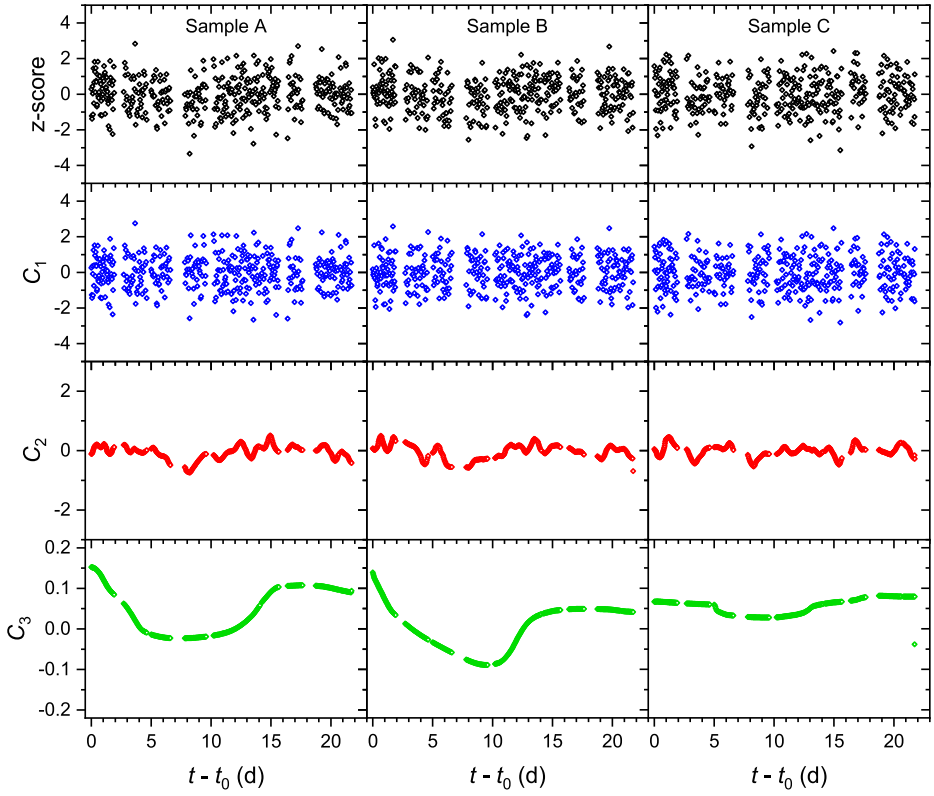

Fig. 10. *Empirical mode decomposition of the residuals to the least-squares fit to samples A, B, and C data sets measured by the HIDEX 300SL liquid scintillation counter. The random statistical component (C_1), a medium-frequency (C_2), and a slow-frequency remainder (C_3) component are shown.*

relationship is not linear. Therefore, the half-life determined from the TDCR correction has not been used in this determination and is used only as an indication of the counting efficiency stability over time.

The uncertainty contribution of the linearity has previously been specified in section 2.4. The uncertainty of the ^{156}Tb and background have been estimated from the average of the propagated uncertainty of these components to the activity at the start and end of the measurement campaign. The uncertainty budget and the estimates of the uncertainties attached to the $u(A)/A$ are given in Table 5. The half-life and its combined standard uncertainty by liquid scintillation counting have been determined as $T_{1/2}(^{155}\text{Tb}) = 5.2344(44)$ d.

4. Discussion

The half-lives determined by the independent techniques of HPGe gamma-ray spectrometry ($T_{1/2} = 5.2349(62)$ d) and liquid scintillation counting using the TDCR method ($T_{1/2} = 5.2344(44)$ d) from two separate productions are in agreement (ζ-score = 0.066) with a relative difference of 0.010%. Assuming that the two determinations are independent, considering different samples and independent techniques used, a weighted mean (WM) of these two determinations gives $T_{1/2}(^{155}\text{Tb}) = 5.2346(36)$ d.

The samples used in these half-life determinations have undergone a combination of radiochemical purification stages and been mass separated at the CERN-MEDICIS facility. This has resulted in highly purified samples that are ideal for half-life measurements and have contributed

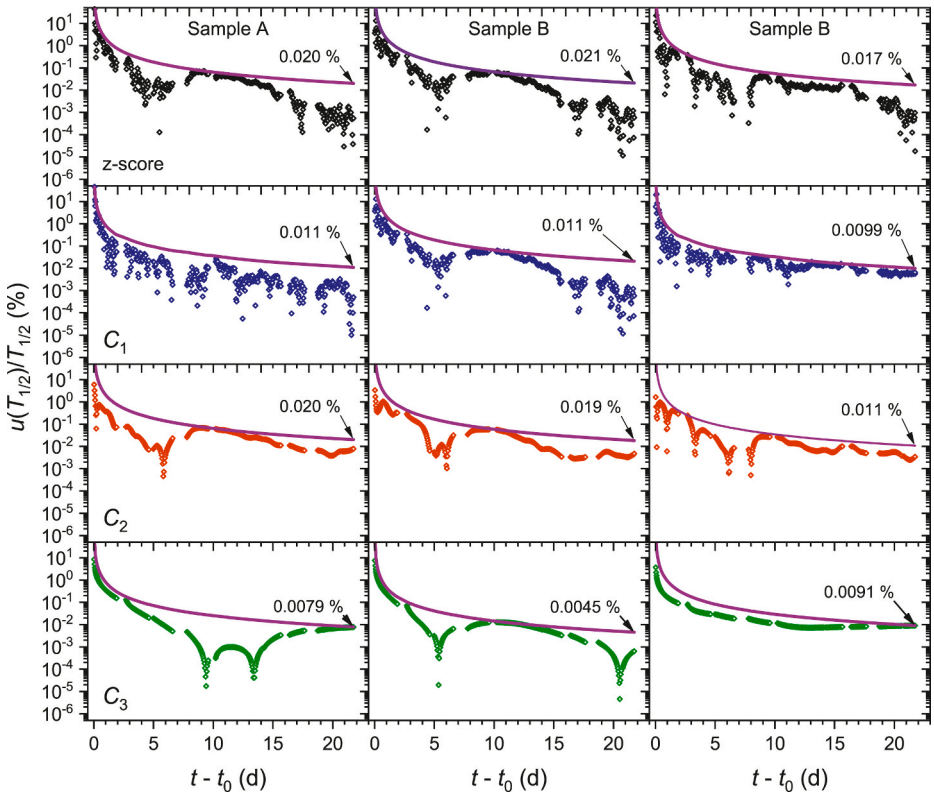

Fig. 11. *Relative uncertainty of the half-life for the decomposition modes C_1, C_2, and C_3 as a function of time for the samples A, B, and C residuals. The purple lines represent their envelope function, with their ultimate uncertainty values indicated.* (For interpretation of the references to colour in this figure legend, the reader is referred to the Web version of this article.)

Table 5
The half-life and uncertainty budget for Liquid scintillation counting, using the TDCR technique, of sample 2.

Component	Sample A				Sample B				Sample C			
	$\frac{\sigma(A)}{A}$	n	Propagation factor	$\frac{\sigma(T_{1/2})}{T_{1/2}}$	$\frac{\sigma(A)}{A}$	n	Propagation factor	$\frac{\sigma(T_{1/2})}{T_{1/2}}$	$\frac{\sigma(A)}{A}$	n	Propagation factor	$\frac{\sigma(T_{1/2})}{T_{1/2}}$
	/%			/%	/%			/%	/%			/%
Standard deviation of residuals	0.15	413	0.0591	0.0088	0.15	413	0.0591	0.0089	0.16	413	0.0591	0.0094
Medium frequency (C_2)	–	–	–	0.020	–	–	–	0.019	–	–	–	0.011
Slow frequency (C_3)	–	–	–	0.0079	–	–	–	0.0045	–	–	–	0.0091
$T_{1/2}$/sample	5.2345(13) d			0.024	5.2342(12) d			0.022	5.23443(90) d			0.017
Standard uncertainty of the weighted mean	–	–	–	0.012								
Stability	0.066	1	0.6950	0.046								
Linearity	0.10	1	0.6950	0.070								
Background correction	0.0069	1	0.6950	0.0048								
^{156}Tb contaminant	0.0041	1	0.6950	0.0029								
$T_{1/2}$	5.2344 (44) d	0.084										

significantly to the precision achieved in this work. The determinations by Toth et al. (1960) and Chu et al. (1970) used samples radiochemically and mass separated but have not quoted the level of the purity of the samples measured for comparison.

The half-life determined in this work and those in the previously reported are shown in Fig. 12. A 1.6% relative difference to the previously most precise value reported by Chu et al. (1970) is observed. Though due to the standard uncertainty (1.1%) attributed by Chu et al. (1970) the value is not statistically discrepant (ζ-score = 1.4). The precision quoted for the half-life determination in this work is more than one order of magnitude more precise than that previously quoted by Chu et al. (1970). The impact of this improvement in the precision is amply demonstrated in Fig. 13 where the contribution of the standard uncertainty of the half-life propagated to the uncertainty of the activity is reduced from 2.9% to less than 0.2% at $(t - t_0) = 20$ d.

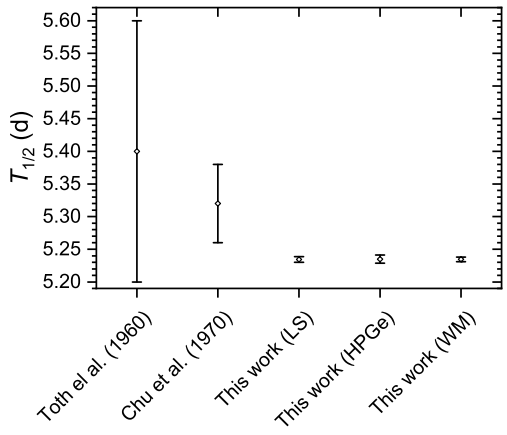

Fig. 12. Comparison of previous literature half-life determinations for ^{155}Tb and those determined in this work.

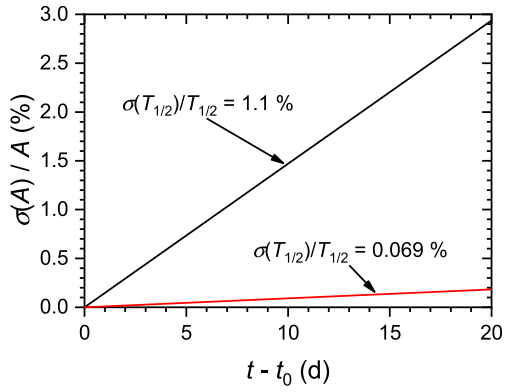

Fig. 13. The uncertainty propagation of the standard uncertainty of the half-life for ^{155}Tb to the uncertainty of the activity (arbitrarily over approximately 3.75 half-lives) for the evaluated half-life (black line) and estimated in this work (red line). (For interpretation of the references to colour in this figure legend, the reader is referred to the Web version of this article.)

5. Conclusion

Prior to the current work, the half-life of the diagnostic radioisotope ^{155}Tb has not been investigated extensively, with a scarcity of determinations and relative standard uncertainties on even the most precise value being inconvenient for radioactive decay corrections even over short time frames. Here, two high purity samples of ^{155}Tb have been produced by a combination of radiochemical separations, and mass separation at CERN-MEDICIS. New half-life determinations have been made of each sample by one of two independent techniques: HPGe gamma-ray spectrometry and liquid scintillation counting. Agreement was found between the two determinations. A new half-life of $T_{1/2}(^{155}\text{Tb}) = 5.2346(36)$ d is reported from the weighted mean of the two determinations. This value has a relative difference of 1.6% to the currently evaluated half-life and has an order of magnitude improvement to the precision.

CRediT authorship contribution statement

S.M. Collins: Writing – review & editing, Writing – original draft, Visualization. **A.P. Robinson:** Writing – review & editing, Supervision, Funding acquisition, Conceptualization. **P. Ivanov:** Methodology, Investigation. **U. Köster:** Writing – review & editing, Resources, Project administration, Investigation, Funding acquisition. **T.E. Cocolios:** Writing – review & editing, Supervision, Resources, Funding acquisition. **B. Russell:** Writing – review & editing, Methodology, Investigation. **B. Webster:** Writing – review & editing, Methodology, Investigation. **A.J. Fenwick:** Writing – review & editing, Project administration, Conceptualization. **C. Duchemin:** Resources, Project administration. **J.P. Ramos:** Writing – review & editing, Resources, Project administration. **E. Chevallay:** Methodology. **U. Jakobsson:** Writing – review & editing, Project administration. **S. Stegemann:** Resources, Project administration. **P.H. Regan:** Writing – review & editing, Supervision. **T. Stora:** Project administration, Funding acquisition.

Declaration of competing interest

The authors declare that they have no known competing financial interests or personal relationships that could have appeared to influence the work reported in this paper.

Data availability

Data will be made available on request.

Acknowledgments

The authors would like to thank Dr. Stefaan Pommé for providing the software for performing the empirical decompositions. The authors would also like to thank Andy Pearce and Dr Robert Shearman for constructive discussions regarding the liquid scintillation analysis. The work performed at NPL was supported by the National Measurements System Programmes Unit of the UK's Department for Business, Energy, and Industrial Strategy and the European Union's Horizon 2020 research and innovation programme under grant agreement No 101008571 (PRISMAP – The European medical radionuclides programme). P. H. Regan also acknowledges funding from the UK Science and Technologies Facilities Council (grant numbers ST/P005314/1 and ST/V001108/1). Collections at CERN-MEDICIS were supported by FWO-Flanders (Belgium).

References

Bé, M.M., Chisté, V., Dulieu, C., Browne, E., Chechev, V., Kuzmenko, N., Helmer, R., Nichols, A., Schönfeld, E., Dersch, R., 2004. Table of Radionuclides, 2–, pp. 151–242. Monographie BIPM-5.

Bé, M.M., Chisté, V., Dulieu, C., Browne, E., Chechev, V., Kuzmenko, N., Kondev, F., Luca, A., Galan, M., Pearce, A., 2008. Table of Radionuclides, vol. 4, pp. 133–252. BIPM, Sevres, 16.

Bobin, C., Bouchard, J., Chisté, V., Collins, S.M., Dryák, P., Fenwick, A., Keightley, J., Lépy, M.-C., Lourenço, V., Robinson, A.P., 2019. Activity measurements and determination of nuclear decay data of ^{166}Ho in the MRTDosimetry project. Appl. Radiat. Isot. 153, 108826.

Broda, R., Cassette, P., Kossert, K., 2007. Radionuclide metrology using liquid scintillation counting. Metrologia 44, S36.

Cavaier, R.F., Haddad, F., Sounalet, T., Stora, T., Zahi, I., 2017. Terbium radionuclides for theranostics applications: a focus on MEDICIS-PROMED. Phys. Procedia 90, 157–163.

Chu, Y.Y., Franz, E.M., Friedlander, G., 1970. Half-lives and gamma-ray abundances of several rare-earth nuclides. Phys. Rev. C 1, 1826.

Collins, S.M., Pommé, S., Jerome, S.M., Ferreira, K.M., Regan, P.H., Pearce, A.K., 2015. The half-life of ^{227}Th by direct and indirect measurements. Appl. Radiat. Isot. 104, 203–211.

Collins, S.M., Shearman, R., Ivanov, P., Regan, P.H., 2020. The impact of high-energy tailing in high-purity germanium gamma-ray spectrometry on the activity determination of ^{224}Ra using the 241.0 keV emission. Appl. Radiat. Isot. 157, 109021.

Duchemin, C., Ramos, J.P., Stora, T., et al., 2020. CERN-MEDICIS: a unique facility for the production of nonconventional radionuclides for the medical research. In: 11th International Particle Accelerator Conference. https://doi.org/10.18429/JACoW-IPAC2020-THVIR13.

Duchemin, C., Ramos, J.P., Stora, T., Ahmed, E., Aubert, E., Audouin, N., Barbero, E., Barozier, V., Bernardes, A.-P., Bertreix, P., 2021. CERN-MEDICIS: a review since commissioning in 2017. Front. Med. 8, 693682.

Formento-Cavaier, R., Haddad, F., Alliot, C., Sounalet, T., Zahi, I., 2020. New excitation functions for proton induced reactions on natural gadolinium up to 70 MeV with focus on ^{149}Tb production. Nucl. Instrum. Methods Phys. Res. Sect. B Beam Interact. Mater. Atoms 478, 174–181.

Gadelshin, V.M., Barozier, V., Cocolios, T.E., Fedosseev, V.N., Formento-Cavaier, R., Haddad, F., Marsh, B., Marzari, S., Rothe, S., Stora, T., 2020. MELISSA: laser ion source setup at CERN-MEDICIS facility. Blueprint. Nucl. Instrum. Methods Phys. Res. Sect. B Beam Interact. Mater. Atoms 463, 460–463.

Ge, Z., Eronen, T., de Roubin, A., Kostensalo, J., Suhonen, J., Nesterenko, D.A., Beliuskina, O., de Groote, R., Delafosse, C., Geldhof, S., Gins, W., Hukkanen, M., Jokinen, A., Kankainen, A., Kotila, J., Koszorus, A., Moore, I.D., Raggio, A., Rinta-Antila, S., Virtanen, V., Weaver, A.P., Zadvornaya, A., 2022. Direct determination of the atomic mass difference of the pairs ^{76}As-^{76}Se and ^{155}Tb-^{155}Gd rules out ^{76}As and ^{155}Tb as possible candidates for electron (anti) neutrino mass measurements. Phys. Rev. C 106, 015502.

Grau Malonda, A., 1999. Free Parameter Models in Liquid Scintillation Counting. Ciemat.

ISO, 2010. Injection Equipment for Medical Use – Part 1: Ampoules for Injectables. ISO 9187-1:2010.

Kossert, K., Takács, M.P., Nähle, O., 2020. Determination of the activity of ^{225}Ac and of the half-lives of ^{213}Po and ^{225}Ac. Appl. Radiat. Isot. 156, 109020.

Mihelich, J.W., Harmatz, B., Handley, T.H., 1957. Nuclear spectroscopy of neutron-deficient rare earths (Tb through Hf). Phys. Rev. 108, 989–999.

Müller, C., Zhernosekov, K., Köster, U., Johnston, K., Dorrer, H., Hohn, A., van der Walt, N.T., Türler, A., Schibli, R., 2012. A unique matched quadruplet of terbium radioisotopes for PET and SPECT and for alpha- and beta- radionuclide therapy: an in vivo proof-of-concept study with a new receptor-targeted folate derivative. J. Nucl. Med. 53, 1951–1959.

Müller, C., Fischer, E., Behé, M., Köster, U., Dorrer, H., Reber, J., Haller, S., Cohrs, S., Blanc, A., Grünberg, J., Bunka, M., Zhernosekov, K., van der Meulen, N., Johnston, K., Türler, A., Schibli, R., 2014. Future prospects for SPECT imaging using the radiolanthanide terbium-155 - production and preclinical evaluation in tumor-bearing mice. Nucl. Med. Biol. 41 (Suppl. l), e58–e65.

Nica, N., 2019. Nuclear data sheets for A= 155. Nucl. Data Sheets 160, 1–404.

Palenzuela, Y.M., Barozier, V., Chevallay, E., Cocolios, T.E., Duchemin, C., Fernier, P., Huyse, M., Lambert, L., Lopez, R., Marzari, S., 2021. The CERN-MEDICIS isotope separator beamline. Front. Med. 8.

Pommé, S., 2015. The uncertainty of the half-life. Metrologia 52, S51.

Pommé, S., De Hauwere, T., 2020. Derivation of an uncertainty propagation factor for half-life determinations. Appl. Radiat. Isot. 158, 109046.

Pommé, S., Pelczar, K., 2021. Empirical decomposition and error propagation of medium-term instabilities in half-life determinations. Metrologia 58, 035012.

Reich, C., 2009. Nuclear data sheets for A= 154. Nucl. Data Sheets 110, 2257–2532.

Reich, C., 2012. Nuclear data sheets for A= 156. Nucl. Data Sheets 113, 2537–2840.

Toth, K.S., Bjørnholm, S., Jørgensen, M.H., Nielsen, O.B., Skilbreid, O., Svanheden, Å., 1960. The light terbium isotopes a survey of half-lives and γ-ray spectra with the use of mass-separated samples. J. Inorg. Nucl. Chem. 14, 1–7.

Webster, B., Ivanov, P., Russell, B., Collins, S.M., Stora, T., Ramos, J.P., Köster, U., Robinson, A.P., Read, D., 2019. Chemical purification of terbium-155 from pseudo-isobaric impurities in a mass separated source produced at CERN. Sci. Rep. 9, 1–9.

Webster, B.L., 2021. The Chemical Separation of Terbium for Applications in Nuclear Medicine. Doctoral dissertation, Univeristy of Surrey.